

Development of Continuous and Real Time Structural Health Monitoring of Aircraft Primary Structure Through Embedded Carbon Nano Fiber Sensors

M.S. Nisha^a, Dalbir Singh^b and A. Rajaraman

School of Aeronautical Sciences, Hindustan University, Chennai, India

^aCorresponding Author, Email: msnisha@hindustanuniv.ac.in

^bEmail: dsinghcad@gmail.com

ABSTRACT:

In this article, a new approach for structural health monitoring of aircraft primary structure has been dealt with, embedded carbon nano fiber (CNF) sensors. The multi-functional ability of non-conductive Glass Fiber Reinforced Polymers (GFRP) material is enhanced by addition of conductive CNF. An experimental investigation was carried out on bi-directional glass fiber to study the damage sensing capabilities of nano composite through embedded CNF mat-based sensor. In the study, CNF was dispersed in Poly Vinyl Alcohol (PVA) solution, and PVA-CNF sensor mat was developed by using electro-spinning process. This mat was embedded into the GFRP by using vacuum resin transfer moulding process at the design stage. CNF neither increases the weight of the composites nor affects its structural and mechanical properties. CNF sensor mat at various orientation and different wt% was embedded to the GFRP. The fabrications of specimens were done using bi-directional glass fiber with epoxy resin. Incremental tensile loading and unloading were conducted during test, and their corresponding electrical conductivity was monitored. The electrical resistance measurement of the embedded PVA-CNF mat is used to assess the structural weakness during mechanical test. Mechanical loading and the change in electrical resistance were directly correlated. Residual resistance measurements of the CNF mat were monitored during unloading condition for high stress (or strain). Accumulating damage to the composite material was calculated and correlated to the electrical resistance readings. The standard size of the coupons is 250x25x2 mm as per ASTM standard D3039.

KEYWORDS:

Electro-spinning; Electrical conductivity; Structural Health Monitoring; Poly Vinyl Alcohol; Carbon Nano Fiber

CITATION:

M.S. Nisha, D. Singh and A. Rajaraman. 2016. Development of Continuous and Real Time Structural Health Monitoring of Aircraft Primary Structure Through Embedded Carbon Nano Fiber Sensors, *Int. J. Vehicle Structures & Systems*, 8(2), 74-81. doi:10.4273/ijvss.8.2.03

1. Introduction

In the field of aeronautical and automotive industry, GFRPs are widely used mainly due to their high specific mechanical properties. The main focus of the aerospace industry research on multi-functional materials is to reduce their own weight, enhance their mechanical properties and sensing capability. An intelligent Structural Health Monitoring (SHM) system informs the damage development and location of the damage to the engineer adequately. There are different types of sensing techniques namely, acoustic emission sensing [1], piezoelectric sensing, vibration monitoring sensing, optical fiber sensing, and so on, [2-4]. All these techniques are used for monitoring the structure which is made up of different composite materials by embedding different sensors, but each technique has its own merits and demerits. By using embedded piezoelectric sensors in composite structures to detect damages, waves are generated. This is propagated in the composite structures as they need strong propagation of waves to detect even a small damage on the structure.

Damage can also be detected by different methods like ultrasonic lamb waves and guide wave [5] or

impedance spectroscopy [6]; however, such embedded sensor will be affected during manufacturing process cycle. Even though glass fiber is installed in optical fiber sensor for damage detection, loss of transmission signal might occur due to local strain developed in composite structures [7, 8] which will directly affect the fibers coefficient of refraction. If the damage is in the small size (micro), it will not be detected using this technique [9-10]. This forms the main drawback of this technique. The major challenge for developing the nano composites for SHM is in the dispersion of nanoparticles and chemical compatibility with matrix material [11]. In order to overcome this challenge, Carbon Nano Fibers (CNF) were dispersed with polymer solution homogeneously and spun the PVA-CNF using electrospinner. In order to develop next generation sensor, carbon nano-tubes (CNTs), which have many distinct properties, may be explored [12].

The structural and electrical characteristics of CNT make them a promising smart sensor material. The high strength, large elastic modulus, and piezoresistivity (resistance changes with strain) indicate the possibility to make a long continuous sensor to measure strain on structure such as aircraft for SHM. CNTs nano particles

are costly. To overcome the cost effect, in our research work CNF instead CNT was used for investigation and proved that the cost in large scale applications might be reduced [13]. The change in resistance of GFRP composites increased almost linearly in proportion to strain [14]. The design concept of intelligent material for explicit warning of fracture is achieved by hybrid composite materials. To detect occurrence of cracks in concrete at floor slab of the skyscraper or the sensor with preventing function for an invader, carbon fiber and glass fiber reinforced plastics composites are commercially applied for sensing damages.

The methods based on determining the changes in electrical resistance are promising for improving the reliability of materials [15]. There are different processes to produce films of magnetically aligned nanotubes and fibers by using an electrophoretic method [16-17]. The processing consists of dispersing the nanotubes in surfactant, and the polymer solution is fed into the conical outlet in order to get nanofiber. Flow-induced alignment may lead to a preferential orientation of the nanotubes in the mesh that has the form of a mat like ribbon. Unlike carbon fibers, the nanotube fibers can be strongly bent without discontinuous. Its elastic modulus is 10 times higher than the modulus of high-quality bucky paper. Single-fiber composites were fabricated to examine the influence of local nanotube reinforcement on load transfer at the fiber/matrix interface. It indicates that the nanocomposites reinforcement improves interfacial load transfer. Where, selective reinforcement by nanotubes at the fiber/matrix interface likely results in local stiffening of the polymer matrix near the fiber/matrix interface, thus, improving load transfer [17].

The mechanical and electrical properties of a nanoparticle modified glass fibre reinforced epoxy composite, produced via a vacuum assisted resin transfer moulding process (VARTM) are reported in [18-19]. Especially, the carbon nanotube modified matrix systems provide improved mechanical properties as well as an electrical conductivity in the order of 10-2S/m [19], which should be sufficient for stress/strain and damage sensing via electrical conductivity methods as the resulting absolute resistance values measured in the composites are in a measurable range (e.g., several k Ω) [20-21]. In the present work, PVA-CNF mats are embedded in GFRP specimens in order to seek simultaneously the material's response to mechanical load and its sensing capability by means of electrical resistance change in the CNF mat. Various incremental loading - unloading steps have been applied to the manufactured specimens in tension as well as in compression loading. This aims to establish a direct correlation between the mechanical stress and the electrical resistance change of the CNF mat sensor.

Investigation has been made to seek whether this correlation changes with regard to the applied mechanical loads. The mechanical and electrical tests were conducted to assess the potential for stress/strain and damage monitoring and to analyze the output obtained to determine the structural damage. The output of stress/strain and damage monitoring data from different sensors were collected and analyzed the damage intensity to make a reliable sensor position and

orientation, which is also capable of detecting the internal damages on the structure without degrading the mechanical structural failure on the composite.

2. Experimental procedure

2.1. Materials & specimen preparation

The materials used for manufacturing the smart nanocomposites material in the application of SHM systems were (a) CNF of 100nm diameter and 20-200 μ m length as supplied by Sigma-Aldrich (b) Epoxy resin Araldite LY556/hardener HY951 (ratio100:12 parts by weight) as supplied by Huntsman and (c) Glass fiber fabric S2-glass. To prepare the polymer solution with homogeneous mixture of CNF, the stabilizer, solution and the solvent were added directly. 0.1 wt% sodium dodecyl sulphate (SDS), the surfactant used to stabilize CNFs, to the water. Solvent such as water and ethanol of about 40 wt% and 50 wt% was prepared. A few drops of surfactant were added to the solvent and stirred in a magnetic stirrer for 10 minutes. Addition PVA 9.98 wt% (Mw 13,000-23,000, 87-89% hydrolyzed) with temperature of 60°-80° C was maintained, and then well grinded CNFs were dispersed in the solution at a weight fraction of 0.02 wt%. The dispersion was homogenized using a sonication treatment for 180 seconds, which resulted in the separation of individual nano particles from the bundles. Thus, various sample solutions were obtained by varying the individual weight fraction of CNF and PVA in the total polymer solution.

Electrospinning process was used to manufacture the carbon nanofiber mats from the polymer solution. The fiber mat had been manufactured at IIT-Madras (Conducting Polymer Laboratory). The ESPIN-NANO electrospinning apparatus, as shown in Fig. 1, was used for the spinning process. The polymer solution was poured into a syringe, which had needle tip diameter of 0.5mm. The injection rate of 0.5 ml/hr towards the collector drum that rotated at speed range of 240 rpm was maintained. The distance between the needle tip and the collector drum was 17cm. The 26 kV voltages were supplied between the collector drum and the needle. This led to the formation of continuous and randomly oriented PVA-CNF mats on the collector drum from transmitted solution towards the cylindrical collector.

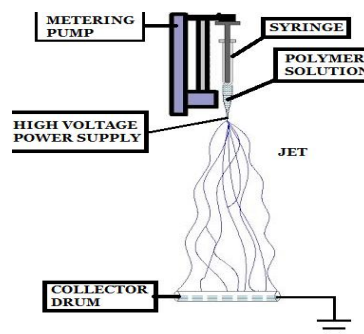


Fig. 1: Schematic diagram of electrospinning

Figs. 2(a) and 2(b) depict the SEM images of CNF and PVA-CNF mat composites respectively. The SEM image of CNF revealed that fibers were of long and uniform shaped. The electrospun PVF-CNF composite, the CNF, were homogenously dispersed uniformly in the

PVA matrix. Similar results were also reported for the PVDF/CNF composites by Sun et al [23]. The synthesized PVA-CNF composites had a diameter of 10µm indicating their micro dimensions. The composites possess a smooth, continuous and interconnected structure that increases the electron-conductivity.

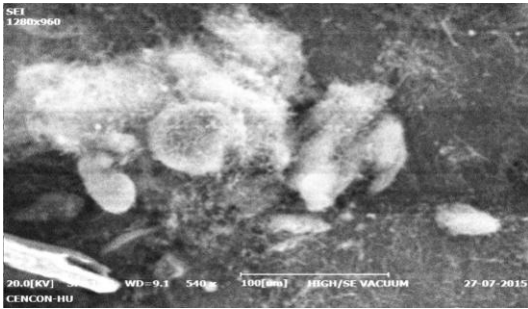


Fig. 2(a): SEM of CNF

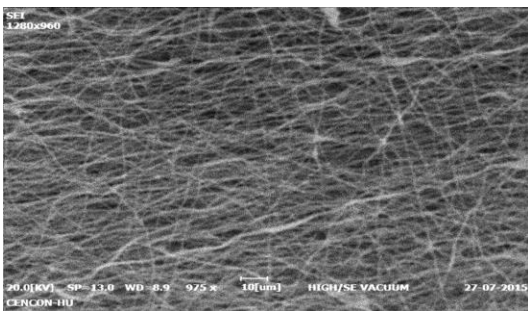


Fig. 2(b): SEM of PVA-CNF fiber mat

For fabricating the glass fiber plate specimens along with the embedded CNF sensors, 10 plies of glass fabric were cut at the required dimensions (300x300 mm) from the GFRP sheet roll. The required number of fiber sensors was cut at the specified length (50x25 mm) in accordance with the specimen needed. The CNF mats were placed between the 9th and last ply as shown in Fig. 3. The specimen dimension of 250x25mm was marked in the plies so that placement of CNF mat sensors can also be marked into each specimen. Conductive silver paste adhesive was used in order to keep the CNF mat in place at the 9th ply, which can be seen in the next layer. After laying up the final ply over the 9th ply, the visible silver paste marks were further covered with the small quantities of silver adhesive to create a means of conductive path to the material's surface and also, where the electrical connections will be placed for recording of the resistance measurements during testing. Fiber sensors were placed in such a way that they were in the middle of each testing specimen to be cut as shown in Fig. 4. The specimens were prepared from the fabricated carbon reinforced composite plate.

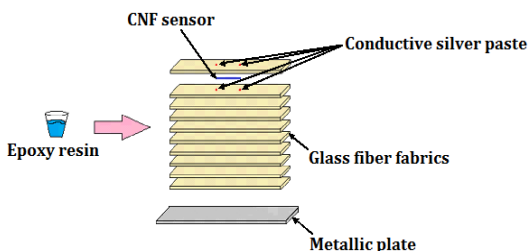


Fig. 3: Pictorial representation of composites plies embedded with CNF sensor

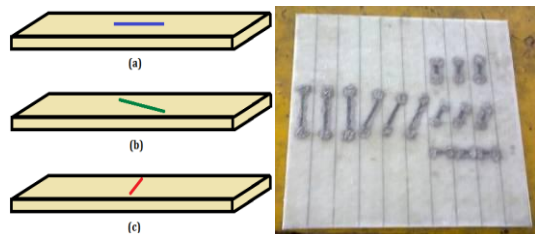


Fig. 4: Pictorial representation of the orientation of the PVA-CNF mat embedded in the composite materials: (a) 0° direction (parallel to the loading), (b) 45° direction (inclined to the loading), (c) 90° direction (horizontal/normal to the loading).

The vacuum resin transfer moulding process had been done at Hindustan University, Padur, Chennai. The 2mm thickness of the laminated composite glass plate, which comprises CNF sensor between the 9th layer and 10th layer, was obtained. The composite plates were cured at ambient temperature for 24 hrs. The standard specimens size of 250x25x2mm as per ASTM standard D3039 [11] were cut from the fabricated laminates size 300x300mm using water-jet cutting to avoid machining defects and to maintain a good surface finish. To facilitate breakage as close as possible to the center of the 150 mm gauge length, two aluminium tabs (size 50x25x1mm) were used on each side of the sample to reduce the grip noise. Aluminium loading tabs were then bonded onto both ends of specimens using a high strength Araldite epoxy adhesive as shown in Fig. 5. The silver paste was applied on the top layer at the two endpoints of the CNF, where the two connective cables had been attached in order to find the resistivity of the fiber with respect to the strain as shown in Fig. 6.

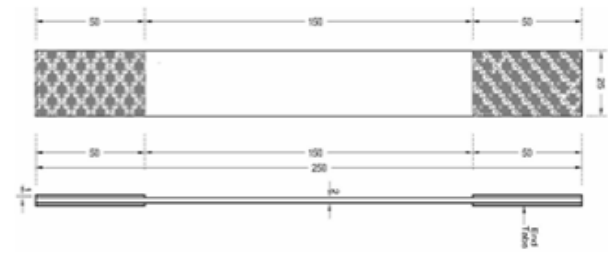


Fig. 5: Specimen geometry and dimensions for tensile test

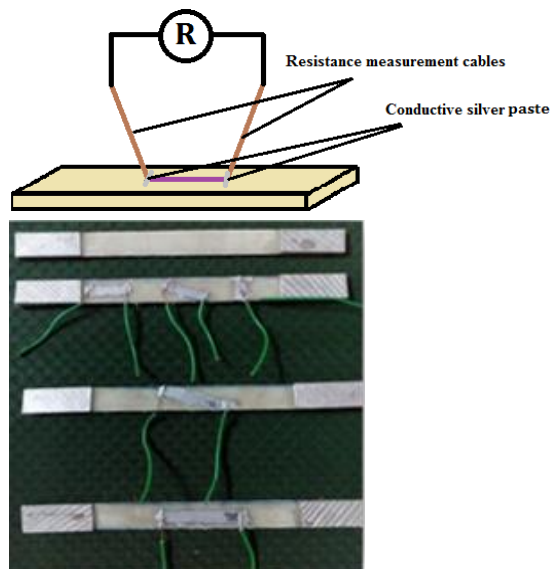


Fig. 6: Electrical resistivity measurement of the sensor

2.2. Testing procedure

ASTM D3039 tensile test specimens, removed from the laminates, were subjected to uniaxial tension using an Instron 3367 universal testing machine. Out of eighteen specimens manufactured, three in each of the following categories were tested:

- 1) Embedding CNF of 0.02 wt % at 0°, 45° and 90°.
- 2) Embedding CNF of 1 wt % at 0°, 45° and 90° bi-directional composite.

In this study, two types of test had been conducted. Initially, monotonic loading fracture was done to determine the fracture point, and then quasi-static incrementing loading-unloading was performed. The corresponding fibers' responses were monitored, and load controlled material testing machine was used for the incremental loading steps to specific levels of tensile fracture stress. All tests were performed using universal testing machine at ambient temperature, and the grips were fixed in such a way that neither bending nor torsion influenced the specimens.

3. Results and discussions

The various incremental loading and unloading results are furnished in Tables 1 and 2, and their graphical representations are shown in Figs. 7 and 8. The four incremental loading and unloading loops for tensile test represent 20%, 35%, 45% and 100% of fracture stress. The direct correlation of mechanical stress and electrical resistance R/Ro of CNF mat are shown in the Figs. 7 and 8. After third loading-unloading conditions, the R/Ro was measured, and it was noticed that incremental growth curve was similar. Then, the mechanical stress and electrical resistance R/Ro were correlated. Under all the four loading conditions, the curve fitting was done by means of a parabolic curve ($R^2=0.8212$). An exponential growth curve fitting was in better correlation as follows,

$$y = Ae^{x/t} \tag{1}$$

The parameters for the exponential growth curve are A and t which were found for varies load conditions and the same are listed in Table 1.

Table 1: Empirical parameters A and t for the exponential growth correlation: 0° orientation of CNF

Specimen	Loading No.	Loading step up to fracture stress (%)	A	t
Sample 0.02 wt % @ 0° orientation	1 st	20	0.00388	31.347
	2 nd	35	0.00555	60.686
	3 rd	45	0.00624	75.089
	4 th	100	0.00967	180.865
Sample 1 wt % @ 0° orientation	1 st	20	0.00119	18.388
	2 nd	35	0.00649	84.937
	3 rd	45	0.01106	128.517
	4 th	100	0.01209	145.249

Table 2: Summary of results with and without CNF

Samples_CNF wt %	Nominal Strain (%)	Nominal Stress (MPa)	Resistance (Ω)	
Without CNF	1.84	206	0	
0.02wt% _CNF	0° Orientation	2.1	256	460
	45° Orientation	2.12	244	116
	90° Orientation	2.06	249	12
1wt%_C NF	0° Orientation	2.6	320	620
	45° Orientation	2.54	316	124
	90° Orientation	2.62	321	34

The first mechanical loading of 20% of fracture stress which is 51 MPa was applied to the specimen, and its corresponding nominal strain was 0.5%. There was a gradual increase in the resistance value of embedded CNF mat, and this was monitored during the 2nd loading and 3rd loading. After the third loading up to 45% of fracture stress, the fourth loading till fracture seemed not to follow the same exponential curve. The graphs clearly show that the 0° orientation of the embedded CNF mat gives better resistance measurement when it experiences axial loading. CNF at 45° and 90° orientations recorded almost identical resistance value with corresponding strain value. Fibers at 45° and 90° orientations recorded lower resistance value when compared to the 0° orientation. Same phenomena was observed for the 1 wt% CNF mat embedded in the GFRP which obtained the highest residual resistance of the fiber during its unloading, and the maximum fracture stress of the composite is increased as shown in the Figs. 8 (a), 8(b) and 8(c) of different orientations of CNF mat.

Between the 3rd and 4th loading, the fracture stress is observed where the exponential co-relation between the stress and R/R0 value is very high, which can be interpreted in two ways either the GFRP are damaged or the embedded CNF mat is damaged. Since the possibilities of damage in GFRPs were obvious, it may be a common damage of matrix crack and deboning of fiber. This may occur during loading condition [22]. There is no shift in correlation was observed during 1st, 2nd, and 3rd loading, but the shift was observed after 3rd loading. Therefore, the initial damage occurs after 45% of fracture stress of the material. The direct correlation between mechanical stress and electrical resistance of different CNF weight percentage (%) is shown in the Figs. 9(a) and 9(b). Higher wt % of CNF concentration in the embedded fiber mat in the GFRP results in maximum stress value when compared to the less concentration of CNF wt % (0.02). The nominal stress and the electrical resistance increased gradually till 260 MPa and further, the material experienced fracture. Meanwhile, the electrical resistance of the 1 wt % of CNF is better when compared to the less concentration of CNF mat.

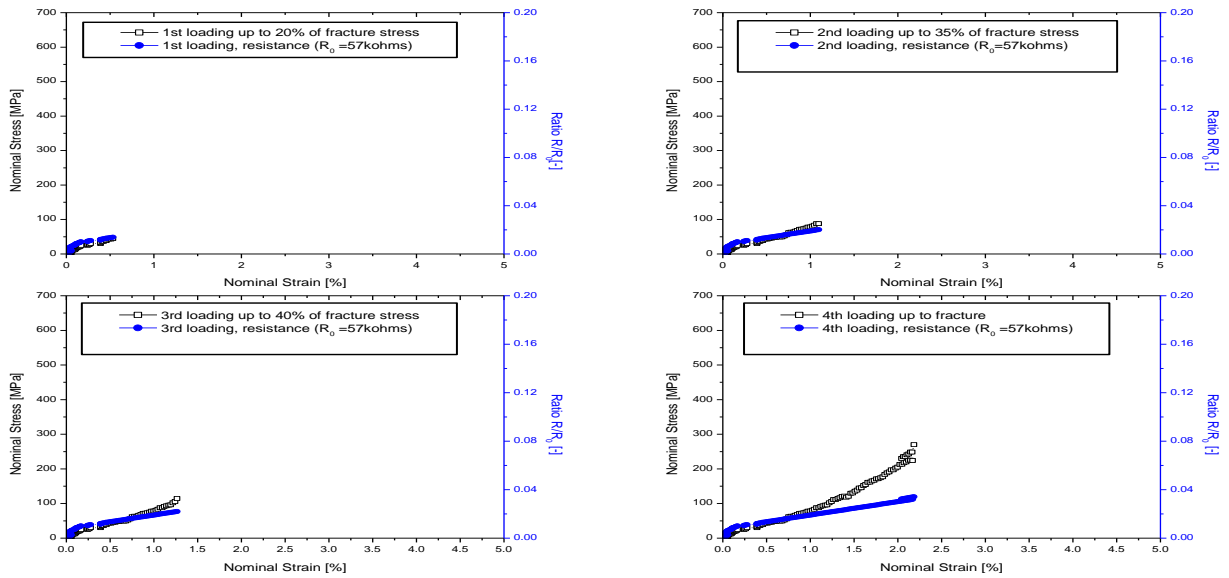


Fig. 7(a): Mechanical tensile and electrical resistance result of GFRP specimen with 0.02 wt % of CNF mat embedded in 0° orientation (parallel to the loading) for 4 different loading conditions

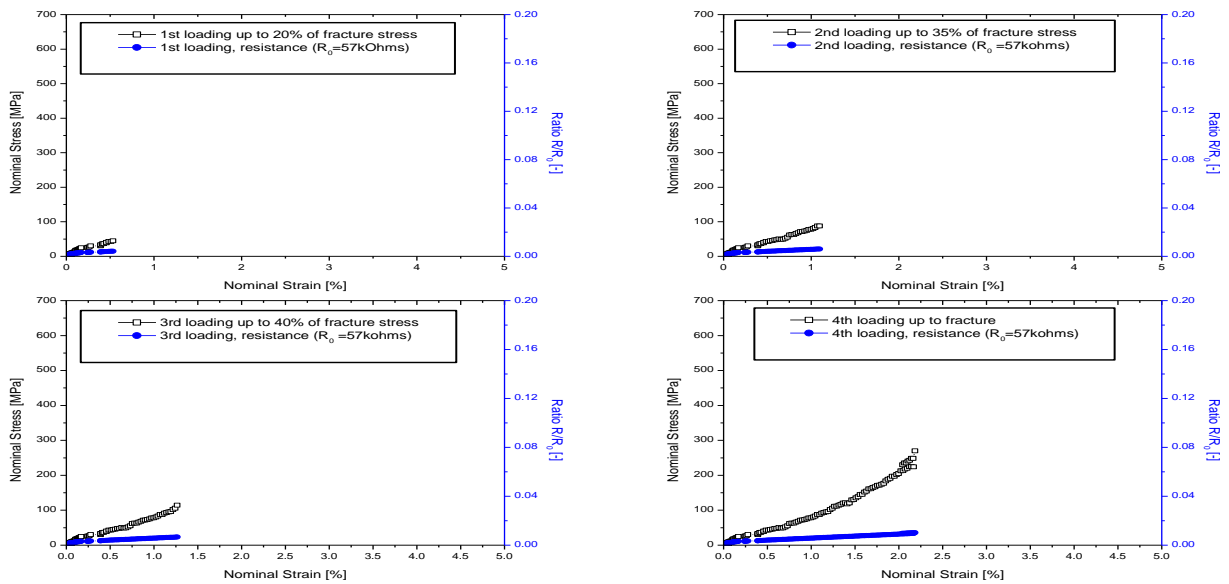


Fig. 7(b): Mechanical tensile and electrical resistance result of GFRP specimen with 0.02 wt % of CNF mats embedded in 45° orientation (inclined to the loading) for 4 different loading conditions

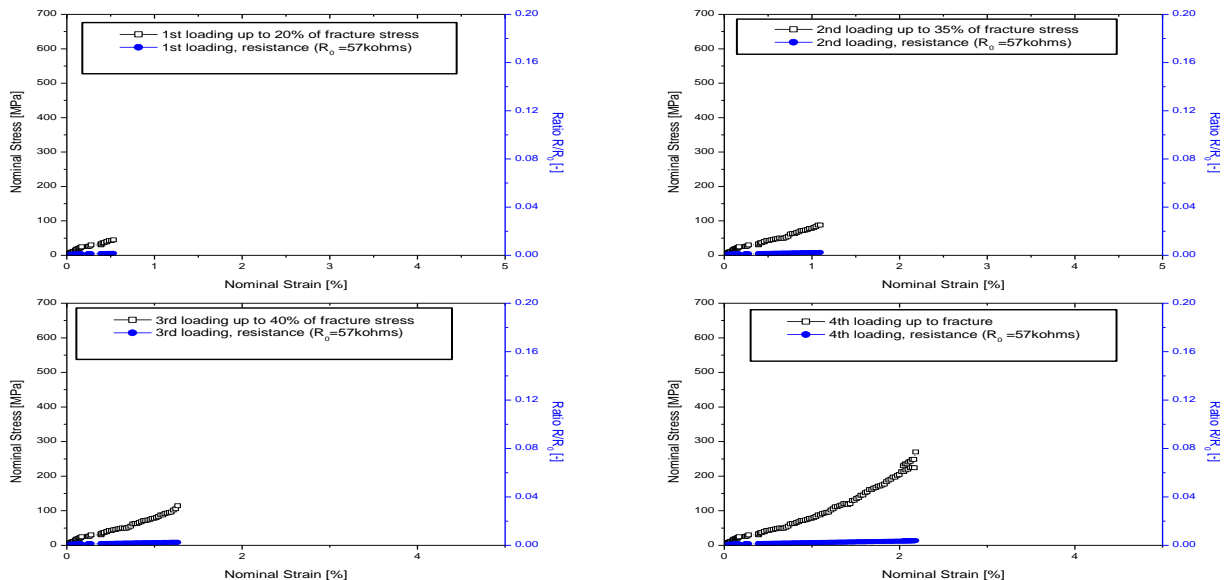


Fig. 7(c): Mechanical tensile and electrical resistance result of GFRP specimen with 0.02 wt % of CNF mat embedded in 90° orientation (horizontal/normal to the loading) for 4 different loading conditions

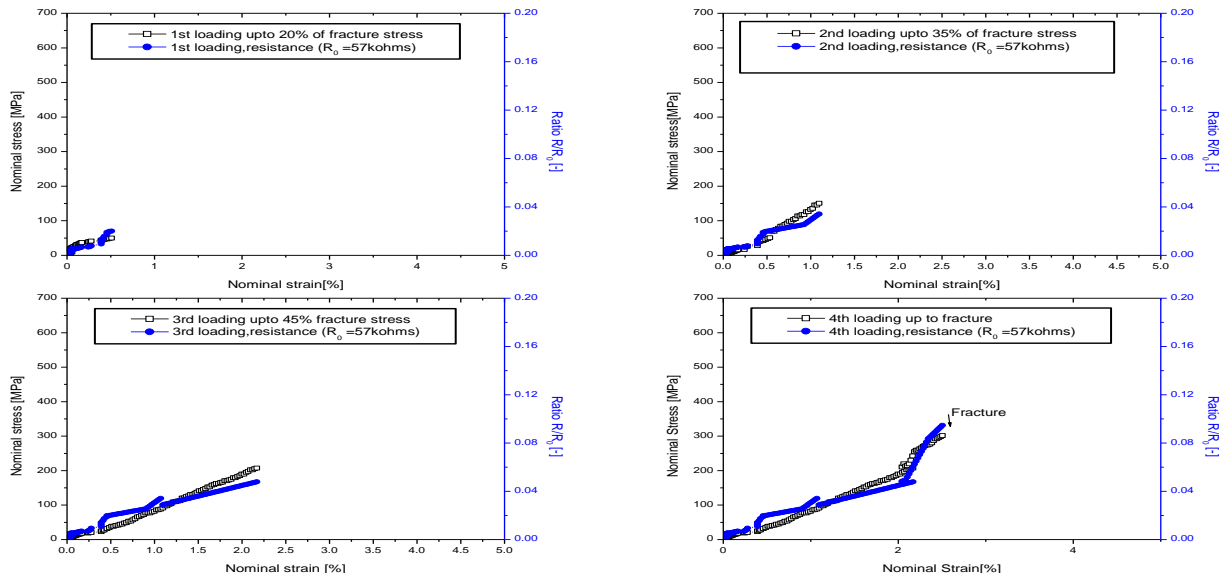


Fig. 8(a): Mechanical tensile and electrical resistance result of GFRP specimen with 1 wt % of CNF mat embedded in 0° orientation (parallel to the loading) for 4 different loading conditions

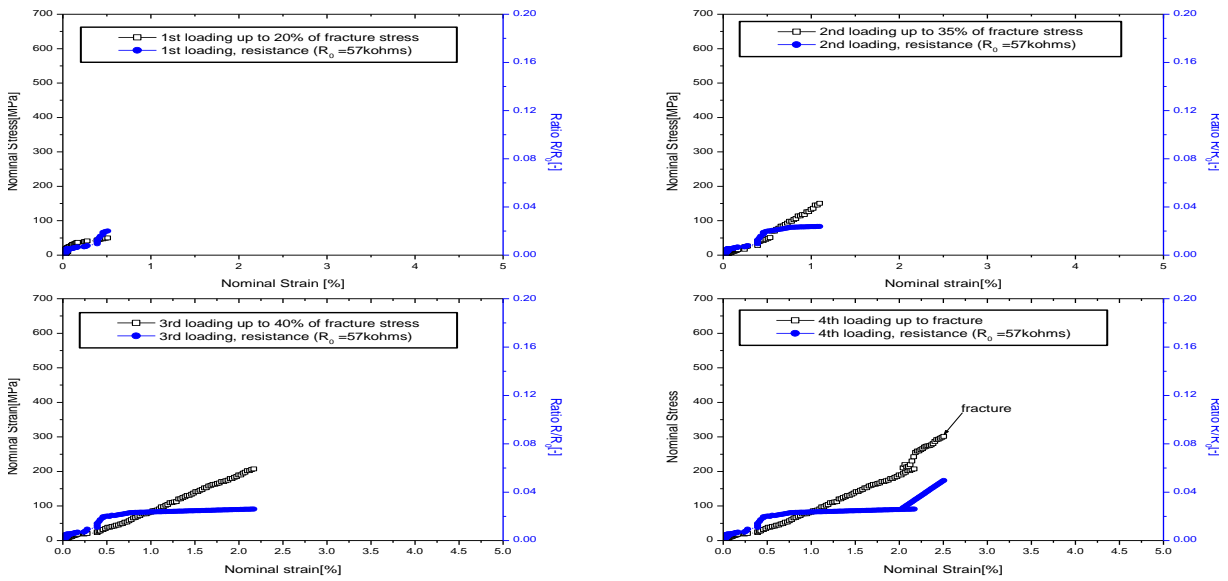


Fig. 8(b): Mechanical tensile and electrical resistance result of GFRP specimen with 1 wt % of CNF mat embedded in 45° orientation (inclined to the loading) for 4 different loading conditions

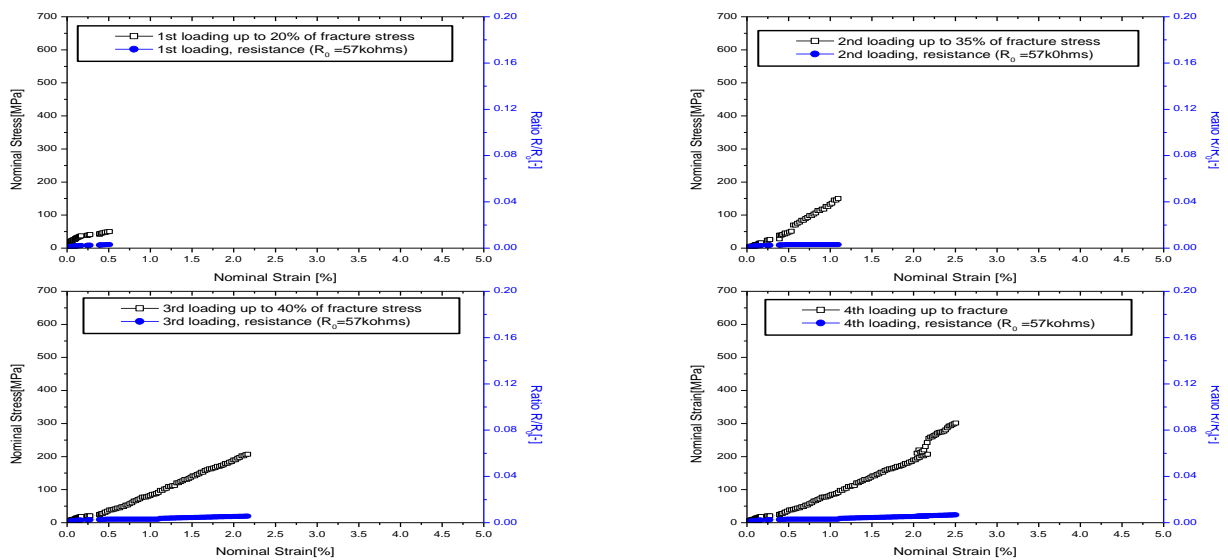


Fig. 8(c): Mechanical tensile and electrical resistance result of GFRP specimen with 1 wt % of CNF mat embedded in 90° orientation (horizontal/normal to the loading) for 4 different loading conditions

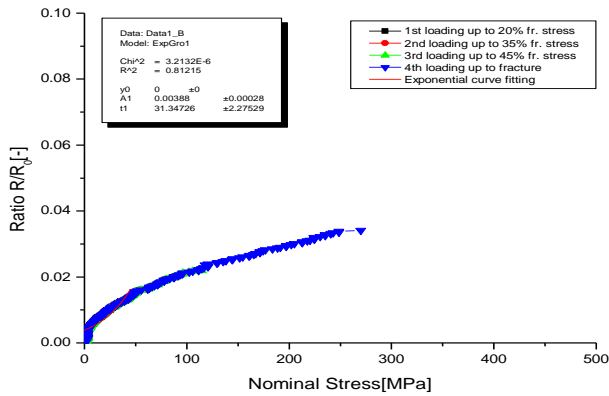


Fig. 9(a): Direct correlation between mechanical stress and electrical resistance measurement for 0.02 wt % of CNF at 0° orientation

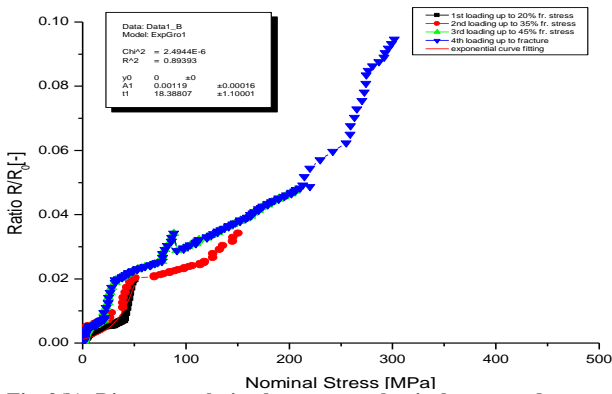


Fig. 9(b): Direct correlation between mechanical stress and electrical resistance measurement for 1 wt % of CNF at 0° orientation

4. Conclusion

For the structural health monitoring system, electrical resistance measurement of the CNF mat had been used by embedding PVA-CNF sensor into the GFRP specimens. The GFRP specimen embedded with CNF sensors presented the same tensile properties with respective coupons without CNF mat. Hence, addition of the CNF mat does not decrease the tensile mechanical properties. Coupons with embedded PVA-CNF mat were subjected to various incremental tensile loading-unloading tests. It could be seen that the applied mechanical stress on the specimen was linearly changed with the electrical resistance of the fiber sensor at different tensile loading cases. Exponential growth curve was well fitted to these parameters. During loading in steps above the level of 40% of the fracture stress of the material which corresponds to the nominal strain of 2.25 % or normal stress of 210 MPa, the direct correlation between the electrical resistance and the stress change.

With respect to the orientation of the CNF mat into the manufactured GFRP, the correlation between the stress and the electrical resistance altered with the same loading condition. The CNF mat with 0° (parallel to the loading condition) orientation has maximum resistance for the same stress compared to the CNF mat oriented at 90° (normal to the load) and 45° orientation falls in between. Coupons with 1 wt % of CNF concentration with 0° orientation give higher nominal stress and electrical resistance than 0.02% CNF. The graphical curves between the mechanical loading and electrical

resistance of the CNF were found to be linear with the applied strain values. Thus, the CNF mat sensor helps to detect the damage of the specimen.

REFERENCES:

- [1] C. Boller, F.K. Chang and Y. Fujino. 2009. *Encyclopedia of Structural Health Monitoring*, John Wiley & Sons Ltd.
- [2] D. Balageas, C. Fritzen and A. Guemes. 2006. *Structural Health Monitoring*, London Newport Beach.
- [3] V. Giurgiutiu. 2008. *Structural Health Monitoring With Piezoelectric Wafer Active Sensors*, Elsevier, Oxford.
- [4] A.S. Kaddour, F.A.R. Al-Salehi, S.T.S. Al-Hassani and M.J. Hinton. 1994. Self-sensing of flexural strain and damage in carbon fiber polymer-matrix composite by electrical resistance measurement, *Composite Science Technology*, 44(13), 377-385. [http://dx.doi.org/10.1016/0266-3538\(94\)90107-4](http://dx.doi.org/10.1016/0266-3538(94)90107-4).
- [5] P. Poulin, B. Vigolo and P. Launois. 2002. Films and fibers of oriented single wall nanotubes, *Carbon*, 40(10), 1741-1749. [http://dx.doi.org/10.1016/S0008-6223\(02\)00042-8](http://dx.doi.org/10.1016/S0008-6223(02)00042-8).
- [6] S.G. Pierce, W.R. Philp, B. Culshaw, A. Gachagan, A.M. Nab, F Lecuyer and G. Hayward. 1996. Surface-bonded optical fibre sensors for the inspection of CFRP plates using ultrasonic Lamb waves, *Smart Mater. Struct.*, 5(6), 776-787. <http://dx.doi.org/10.1088/0964-1726/5/6/007>.
- [7] B. Hofer. 1987. Fibre optic damage detection in composite structures, *Composites*, 18(4), 309-316. [http://dx.doi.org/10.1016/0010-4361\(87\)90294-1](http://dx.doi.org/10.1016/0010-4361(87)90294-1).
- [8] S.R. Waite, R.P. Tatam and A. Jackson. 1988. Use of optical fibre for damage and strain detection in composite materials, *Composites*, 19(6), 435-442. [http://dx.doi.org/10.1016/0010-4361\(88\)90700-8](http://dx.doi.org/10.1016/0010-4361(88)90700-8).
- [9] S. Takeda, Y. Okabe and N. Takeda. 2002. Delamination detection in CFRP laminates with embedded small-diameter fiber bragg grating sensors, *Composites*, 33(7), 971-980. [http://dx.doi.org/10.1016/S1359-835X\(02\)00036-2](http://dx.doi.org/10.1016/S1359-835X(02)00036-2).
- [10] J.M. Park, S.I. Lee, O.Y. Kwon, H.S. Choi and J.H. Lee. 2003. Comparison of nondestructive microfailure evaluation of fiber-optic bragg grating and acoustic emission piezoelectric sensors using fragmentation test, *Composites, Part A*, 34(3), 203-216. [http://dx.doi.org/10.1016/S1359-835X\(03\)00028-9](http://dx.doi.org/10.1016/S1359-835X(03)00028-9).
- [11] F. Hussain. 2006. Review article, polymer-matrix nanocomposites, processing, manufacturing and application: An overview, *J. Comp. Mat.*, 40(17), 1511-1575. <http://dx.doi.org/10.1177/0021998306067321>.
- [12] J.T.W. Yeow, N. Sinha and J. Ma. 2006. Carbon nanotube-based sensors, *J. Nanoscience and Nanotechnology*, 6(3), 573-590. <http://dx.doi.org/10.1166/jnn.2006.121>.
- [13] M.J. Schulz, I. Kang and J.H. Kim. 2006. Introduction to carbon nanotube and nanofiber smart materials, *Composites, Part B*, 37(6), 382-394. <http://dx.doi.org/10.1016/j.compositesb.2006.02.011>.
- [14] A. Chateauminois, S. Bochart, G. Giraud, J.C. Abry and M. Salvia, 1999. In situ detection of damage in CFRP laminates by electrical resistance measurements, *Composites Science Technology*, 59(6), 925-935. [http://dx.doi.org/10.1016/S0266-3538\(98\)00132-8](http://dx.doi.org/10.1016/S0266-3538(98)00132-8).
- [15] N. Muto, Y. Arai, H. Matsubara, H. Yanagida, M. Sugita, T. Nakatsuji and S.G. Shin, 2001. Hybrid composites with self-diagnosing function for preventing fatal fracture,

- Composites Science and Technology*, 61(6), 875-883. [http://dx.doi.org/10.1016/S0266-3538\(00\)00165-2](http://dx.doi.org/10.1016/S0266-3538(00)00165-2)
- [16] C. Jurnet, B. Vigolo and A. Penicaud, 2000. Macroscopic fibers and ribbons of oriented carbon nanotubes, *Science*, 290(5495), 1331-1334.
- [17] T.W. Chou, E.T. Thostenson, W.Z. Li, D.Z. Wang, and Z.F. Ren. 2002. Carbon nanotube/Carbonfiber hybrid multiscale composites, *J. Applied Physics*, 91(9), 6034-7.
- [18] F.H. Gojny, M.H.G. Wichmann, B. Fiedler, W. Bauhofer and K. Schulte. 2005. Influence of nano-modification on the mechanical and electrical properties of conventional fibre-reinforced composites, *Composites A*, 36(11), 1525-1535. <http://dx.doi.org/10.1016/j.compositesa.2005.02.007>.
- [19] M.H.G. Wichmann, J. Sumfleth, F.H. Gojny, M. Quaresimin, B. Fiedler and K. Schulte. 2006. Glass-fibre-reinforced composites with enhanced mechanical and electrical properties - Benefits and limitations of a nanoparticle modified matrix, *Eng. Fract. Mech.*, 73(16), 2346-2359. <http://dx.doi.org/10.1016/j.engfracmech.2006.05.015>.
- [20] B. Fiedler, F.H. Gojny, M.H.G. Wichmann, M.C.M. Nolte and K. Schulte. 2006. Fundamental aspects of nano-reinforced composites, *Composite Science Tech.*, 66(16), 3115-3125. <http://dx.doi.org/10.1016/j.compscitech.2005.01.014>.
- [21] B. Fiedler, F.H. Gojny, M.H.G. Wichmann, W. Bauhofer and K. Schulte. 2004. Can carbon nanotubes be used to sense damage in composites?, *Ann. Chim. Sci. Mater.*, 29(6), 81-94. <http://dx.doi.org/10.3166/acsm.29.6.81-94>.
- [22] N.D. Alexopoulos, C. Bartholome, P. Poulin and Z. M.Riga. 2010. Structural health monitoring of glass fiber reinforced composites using embedded carbon nanotube (CNT) fibers, *Composite Science Tech.*, 70(2), 260-271. <http://dx.doi.org/10.1016/j.compscitech.2009.10.017>.
- [23] L.L. Sun. 2010. Achieving very high fraction of b-crystal PVDF and PVDF/CNF composites and their effect on AC conductivity and microstructure through a stretching process, *European Polymer J.*, 46(11), 2112-2119. <http://dx.doi.org/10.1016/j.eurpolymj.2010.09.003>.